JCI insight

RESEARCH ARTICLE

Mfge8 regulates enterocyte lipid storage by promoting enterocyte triglyceride hydrolase activity

Amin Khalifeh-Soltani,[1,2,3] Deepti Gupta,[1,2,3] Arnold Ha,[1,2] Jahangir Iqbal,[4] Mahmood Hussain,[4] Michael J. Podolsky,[1,2,3] and Kamran Atabai[1,2,3]

[1]Department of Medicine, [2]Cardiovascular Research Institute, [3]Lung Biology Center, University of California, San Francisco, San Francisco, California, USA. [4]Departments of Cell Biology and Pediatrics, SUNY Downstate Medical Center, Brooklyn, New York, USA.

The small intestine has an underappreciated role as a lipid storage organ. Under conditions of high dietary fat intake, enterocytes can minimize the extent of postprandial lipemia by storing newly absorbed dietary fat in cytoplasmic lipid droplets. Lipid droplets can be subsequently mobilized for the production of chylomicrons. The mechanisms that regulate this process are poorly understood. We report here that the milk protein Mfge8 regulates hydrolysis of cytoplasmic lipid droplets in enterocytes after interacting with the αvβ3 and αvβ5 integrins. Mice deficient in Mfge8 or the αvβ3 and αvβ5 integrins accumulate excess cytoplasmic lipid droplets after a fat challenge. Mechanistically, interruption of the Mfge8-integrin axis leads to impaired enterocyte intracellular triglyceride hydrolase activity in vitro and in vivo. Furthermore, Mfge8 increases triglyceride hydrolase activity through a PI3 kinase/mTORC2–dependent signaling pathway. These data identify a key role for Mfge8 and the αvβ3 and αvβ5 integrins in regulating enterocyte lipid processing.

Introduction

Intestinal lipid homeostasis has important implications for the development of obesity and atherosclerotic heart disease (1, 2). In addition to absorbing nutrients, the small intestine is a lipid storage organ that regulates the extent of postprandial serum lipid levels by modulating chylomicron production. Under conditions of high dietary fat intake, the intestine stores triglycerides (TGs) in cytoplasmic lipid droplets (3). Lipid droplets protect the cell from the toxicity of high intracellular free fatty acid (FFA) concentrations and provide a rapid source of stored TG that can be hydrolyzed for chylomicron production in response to food ingestion (3).

Enterocyte storage of dietary fats as cytoplasmic lipid droplets also provides a mechanism for regulating the amount of chylomicron secretion after a meal. Inhibiting the extent of chylomicron secretion is important since the degree of postprandial lipemia (secondary to chylomicron secretion) has a stronger correlation with coronary artery disease than fasting serum lipid levels (4). In obesity, intestinal insulin resistance removes the suppressive effect of insulin on chylomicron production, leading to exaggerated postprandial lipemia (5). Interestingly, the immediate postprandial elevation in serum lipid levels in humans consists primarily of TGs derived from lipid droplets originating from previous meals when each meal is high in fat content (6). These data suggest that ingestion of food triggers the enterocyte to liberate FFAs from TGs in cytoplasmic lipid droplets for chylomicron production and export. The mechanisms that coordinate this process are poorly understood.

We have previously shown that the integrin ligand milk fat globule epidermal growth factor–like 8 (Mfge8) (7, 8) regulates the absorption of dietary fat by enterocytes through binding of the αvβ3 and αvβ5 integrins (9). Integrin ligation by Mfge8 activates a PI3 kinase/mTORC2/PKCζ–dependent pathway that results in cellular uptake of FFAs. We have also recently shown that Mfge8 promotes nutrient absorption by slowing gastrointestinal transit time through ligation of the α8β1 integrin (10). We were interested in examining whether in addition to promoting fatty acid and nutrient uptake, the Mfge8-integrin axis regulates intracellular lipid processing. We report here that Mfge8 and the αvβ3 and αvβ5 integrins coordinate release of FFAs from cytoplasmic lipid droplets in enterocytes by increasing intracellular TG hydrolase activity. This pathway provides a previously unappreciated mechanism linking the absorption of dietary fats with the hydrolysis of intracellular lipid stores in preparation for postprandial chylomicron secretion.

Conflict of interest: The authors have declared that no conflict of interest exists.

Submitted: March 4, 2016
Accepted: October 5, 2016
Published: November 3, 2016

Reference information:
JCI Insight. 2016;1(18):e87418.
doi:10.1172/jci.insight.87418.

Results

We have previously reported that Mfge8 promotes enterocyte FFA uptake and that serum TG levels in *Mfge8*$^{-/-}$ mice are significantly reduced after an olive oil gavage (9). FFAs released from dietary fat in the intestinal lumen are absorbed by enterocytes and trafficked to the endoplasmic reticulum (ER) where they are esterified into TG (11–14). TG can then be stored as part of cytoplasmic lipid droplets or packaged as part of chylomicrons. Cytoplasmic lipid droplets are subsequently hydrolyzed, releasing FFAs that are re-esterified into TG, and incorporated into chylomicrons for secretion into the lymphatic system (15–19). The reduction in serum TG after olive oil gavage seen in *Mfge8*$^{-/-}$ mice may therefore be the result of a defect anywhere along this pathway.

To examine whether disruption of the Mfge8-integrin axis perturbs intracellular lipid processing by enterocytes, we quantified enterocyte TG content after olive oil gavage in *Mfge8*$^{-/-}$ and mice deficient in both the αvβ3 and αvβ5 integrins (*αvβ3*$^{-/-}$ *αvβ5*$^{-/-}$ mice, hereafter referred to as *αvβ3/αvβ5*$^{-/-}$ mice). In both mouse lines, enterocyte TG content was significantly increased after olive oil gavage despite a reduction in serum TG (Figure 1, A–C, the serum data for *Mfge8*$^{-/-}$ mice was previously reported in ref. 9). The elevated TG content after olive oil gavage contrasts with our previously reported reduction in enterocyte TG content in *Mfge8*$^{-/-}$ mice that have not had administration of an acute fat load (9). *Mfge8*$^{-/-}$ and *αvβ3/αvβ5*$^{-/-}$ mice also had increased stool TG levels at baseline and after olive oil gavage as compared with WT controls (Figure 1, D and E).

To verify that the reduced serum TG represents reduced secretion of absorbed dietary fats, we gavaged *Mfge8*$^{-/-}$ and *αvβ3/αvβ5*$^{-/-}$ mice with ^{14}C-triolein and measured the radioactive signal in the proximal jejunum 2 hours after gavage and in the serum at multiple time points after gavage. Both *Mfge8*$^{-/-}$ and *αvβ3/αvβ5*$^{-/-}$ mice had significantly increased radioactive signal in the jejunum (Figure 1F) and significantly reduced radioactive signal in the serum (Figure 1G) as compared with WT controls. Oil Red O staining of intestinal sections 2 hours after olive oil gavage demonstrated a dramatic increase in cytoplasmic lipid droplets within enterocytes of *Mfge8*$^{-/-}$ and *αvβ3/αvβ5*$^{-/-}$ mice as compared with WT controls (Figure 1H). To further prove that lipid droplets were cytoplasmic, we stained tissue sections 30 minutes after olive oil gavage with perilipin 3 (TIP47), a protein that is expressed in enterocytes and coats cytoplasmic lipid droplets after a high-fat challenge (20). Perilipin 3 staining was increased in sections from *Mfge8*$^{-/-}$ mice as compared with WT controls (Figure 1I). These data indicate that disruption of the Mfge8-integrin axis results in enterocyte accumulation of intracellular TG likely as cytoplasmic lipid droplets.

To examine whether chronic intake of a fat-rich diet also led to retention of lipid droplets with disruption of the Mfge8-integrin axis, we placed 8-week-old *Mfge8*$^{-/-}$, *αvβ3/αvβ5*$^{-/-}$, and WT mice on a high-fat diet (HFD) or control diet (CD) for 3 weeks, after which we fasted mice for 12 hours prior to evaluating intestinal TG content. Oil Red O staining of sections from WT mice on an HFD was similar to those from WT mice on a CD after the 12-hour fast. However, *Mfge8*$^{-/-}$ and *αvβ3/αvβ5*$^{-/-}$ mice on an HFD had an increase in cytoplasmic lipid droplets (Figure 2A). *Mfge8*$^{-/-}$ and *αvβ3/αvβ5*$^{-/-}$ mice also had significantly elevated jejunal TG content (Figure 2, B and C). These data indicate that interruption of the Mfge8-integrin axis results in accumulation of intracellular TG in enterocytes when mice are challenged with chronic intake of a fat-rich diet.

Incorporation of absorbed dietary fat into chylomicrons involves a series of steps by which FFAs are incorporated into TG in the endoplasmic reticulum and subsequently packaged with phospholipids, lipoproteins, and cholesterol esters to form chylomicrons. Microsomal triglyceride transfer protein (MTTP) is the key enzyme required for chylomicron assembly. We therefore evaluated MTTP activity in the jejunum and liver of *Mfge8*$^{-/-}$ and *αvβ3/αvβ5*$^{-/-}$ mice 2 hours after olive oil gavage and also in mice on a CD and HFD. MTTP activity was not significantly reduced in *Mfge8*$^{-/-}$ and *αvβ3/αvβ5*$^{-/-}$ mice (Supplemental Figure 1, A–F). Furthermore, expression of ApoB, the critical apoprotein for chylomicron assembly protein, was unchanged 2 hours after olive oil gavage in the jejunum of *Mfge8*$^{-/-}$ and *αvβ3/αvβ5*$^{-/-}$ mice (Supplemental Figure 1G). These data suggest that Mfge8 deficiency does not affect chylomicron assembly.

We next isolated enterocyte RNA from *Mfge8*$^{-/-}$ and WT mice on a CD and HFD and evaluated expression of critical mediators of TG synthesis, hydrolysis, and secretion. We evaluated expression of MGAT1, MGAT2, DGAT1, DGAT2, ATGL, HSL, CGI-58, TGH, ApoB, MTP, Schekman's factor, and Lehner's TGH by real-time PCR (Supplemental Figure 2, A and B). While there were no major differences in either mice on a CD or HFD for most of these molecules, we did see a statistically significant increase in DGAT2 expression in *Mfge8*$^{-/-}$ mice on an HFD as well as a trend towards increased DGAT2 expression in *Mfge8*$^{-/-}$ mice on a CD.

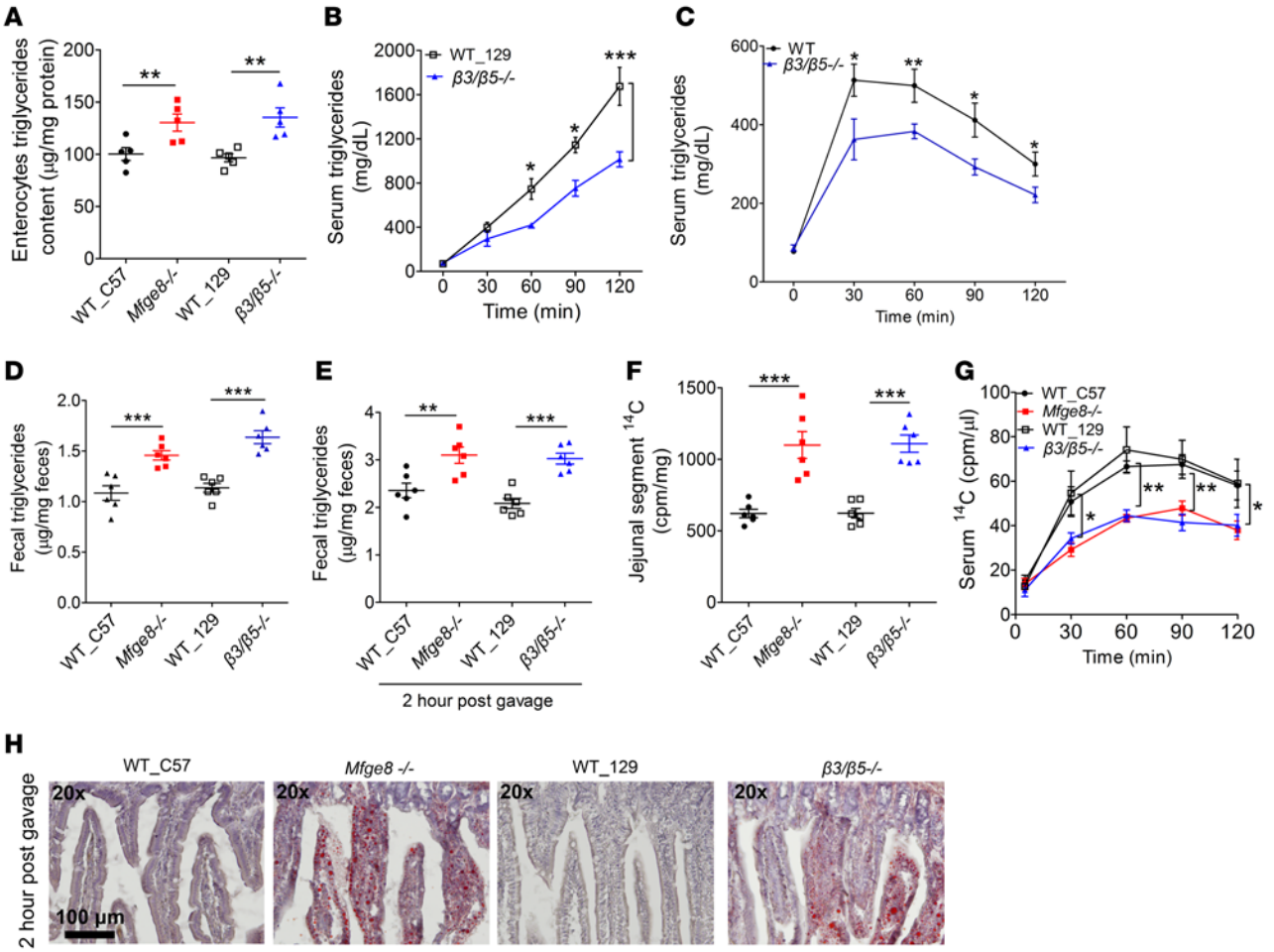

Figure 1. Accumulation of intracellular triglyceride (TG) in *Mfge8*$^{-/-}$ and *αvβ3/αvβ5*$^{-/-}$ mice after a dietary fat challenge. (**A**) TG content in primary enterocytes isolated from the proximal jejunum 2 hours after olive oil gavage. $n = 5$. (**B** and **C**) Serum TG concentrations over time after olive oil gavage in the presence (**B**) or absence (**C**) of i.p. administration of the lipoprotein lipase inhibitor Triton WR-1339. $n = 5$. (**D** and **E**) Baseline fecal TGs (**D**) and fecal TGs 2 hours after olive oil gavage (**E**). $n = 5$–6. (**F** and **G**) Radiolabel signal in proximal jejunal segments (**F**) or in the serum (**G**) 2 hours after gavage with ^{14}C-triolein. $n = 4$–5. (**H**) Oil Red O staining of proximal jejunal segments 2 hours after olive oil gavage. (**I**) Jejunal sections obtained 30 minutes after olive oil gavage were stained with anti–perilipin 3 antibody. Female mice were used in all panels. $^{*}P < 0.05$, $^{**}P < 0.01$, $^{***}P < 0.001$. Paired data were analyzed by Student's *t* test and group data were analyzed by 1-way ANOVA followed by a post-hoc Bonferroni test for multiple comparisons and expressed as the mean ± SEM.

Our data demonstrating an increase in lipid droplets by Oil Red O and perilipin 3 staining strongly suggest retention of TGs in the cytoplasm with disruption of the Mfge8-integrin axis. As a complementary method evaluating the location of retained TG, we gavaged *Mfge8*$^{-/-}$ and *αvβ3/αvβ5*$^{-/-}$ mice with ^{14}C-triolein, isolated the proximal jejunum, and separated the microsomal versus cytosolic fractions (Supplemental Figure 3, A and B). We then measured radioactivity in each fraction. In *Mfge8*$^{-/-}$ and *αvβ3/αvβ5*$^{-/-}$ mice there was a significant increase in the radiolabel in the cytosolic compartment with no difference in the microsomal compartments as compared with WT controls (Figure 3, A and B). To quantify incorporation

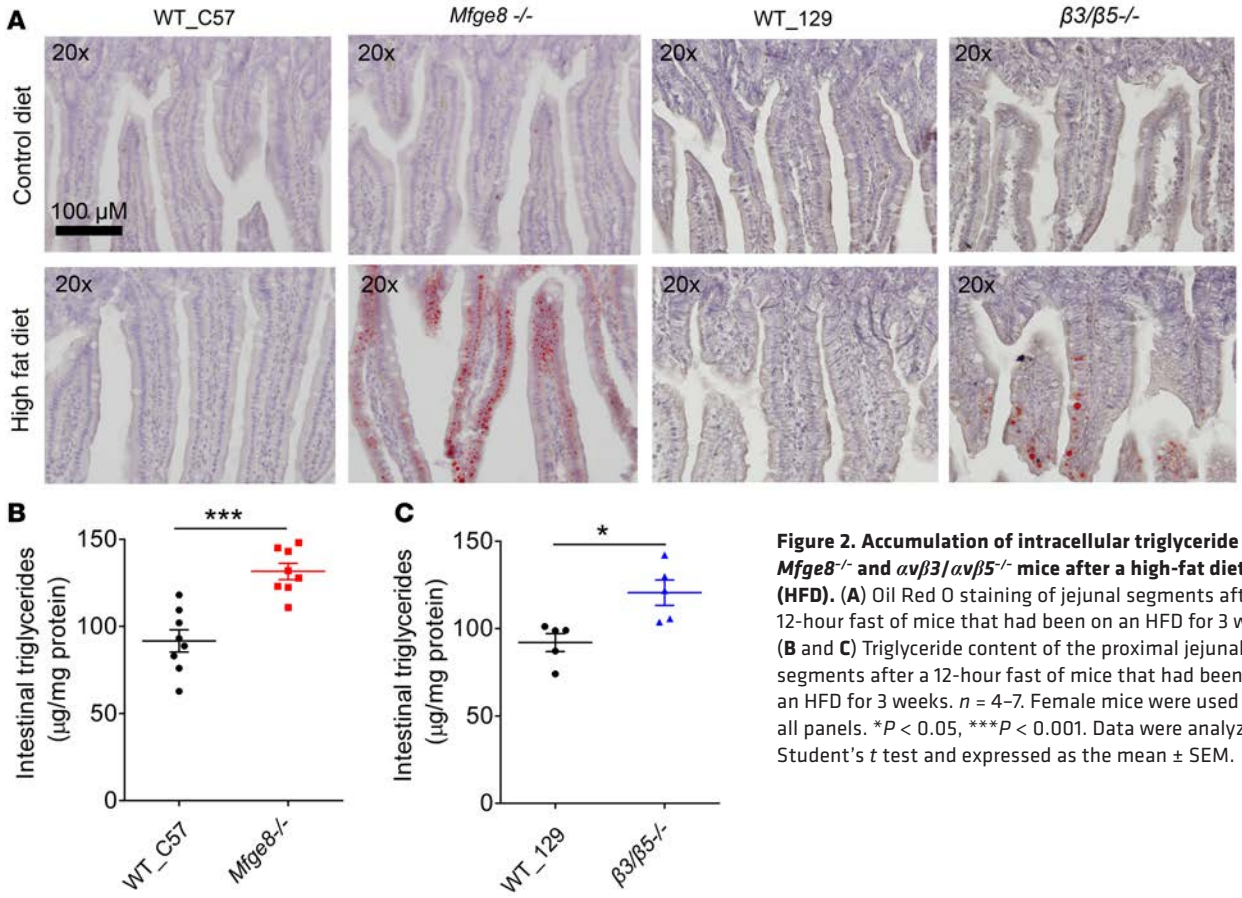

Figure 2. Accumulation of intracellular triglyceride in *Mfge8*$^{-/-}$ and *αvβ3/αvβ5*$^{-/-}$ mice after a high-fat diet (HFD). (**A**) Oil Red O staining of jejunal segments after a 12-hour fast of mice that had been on an HFD for 3 weeks. (**B** and **C**) Triglyceride content of the proximal jejunal segments after a 12-hour fast of mice that had been on an HFD for 3 weeks. n = 4–7. Female mice were used for all panels. $^*P < 0.05$, $^{***}P < 0.001$. Data were analyzed by Student's t test and expressed as the mean ± SEM.

of radiolabel (^{14}C) in different intracellular lipid species after ^{14}C-triolein gavage, we performed TLC of jejunal enterocytes isolated 2 hours after ^{14}C-triolein gavage (14). Enterocytes from *Mfge8*$^{-/-}$ and *αvβ3/αvβ5*$^{-/-}$ mice had significantly greater radiolabeled diacylglycerol (DAG) and TG and significantly less radiolabeled FFAs (Figure 3C) as compared with WT controls.

Next we isolated primary enterocytes from *Mfge8*$^{-/-}$ and *αvβ3/αvβ5*$^{-/-}$mice, incubated them with bile salt micelles containing ^{14}C–oleic acid for 30 minutes, washed off the bile salt micelles, and subsequently incubated cells with fresh media for 1.5 hours to monitor processing of intracellular lipids. Of note, primary enterocyte viability after isolation, as measured by flow cytometry after annexin V and propidium iodide (PI) staining, was greater than 90% (Supplemental Figure 4, A and B). We then measured radiolabel content of lipid species within enterocytes after resolving by TLC (14). Similar to our in vivo data, enterocytes had an increase in ^{14}C-labeled DAG and TG (Figure 3D). Importantly, despite this increase in radiolabeled neutral lipids, the concentration of ^{14}C-labeled FFAs was reduced, consistent with our previously published work (9). We also quantified the appearance of the ^{14}C label in secreted TG in the media at the end of the 2-hour assay. Media from *Mfge8*$^{-/-}$ and *αvβ3/αvβ5*$^{-/-}$ enterocytes had significantly less ^{14}C-labeled TG (Figure 3E).

We then performed time course experiments to characterize uptake, cellular assimilation, and secretion of TG in primary enterocytes after a 30-minute incubation (pulse) with ^{14}C–oleic acid micelles followed by washing off the micelles and a 2-hour incubation with fresh media (chase). We evaluated radiolabeled TG in cellular pellets of enterocytes by TLC at all time points. We also evaluated radioactivity in the media during the 30-minute incubation with ^{14}C–oleic acid micelles as well as radiolabeled TG secreted into the media by TLC 0, 30, 60, and 120 minutes after washing off the ^{14}C–oleic acid micelles (Figure 3, F–H). The TG content in the cellular pellets was less in *Mfge8*$^{-/-}$ and *αvβ3/αvβ5*$^{-/-}$ enterocytes beginning 15 minutes after incubation with ^{14}C–oleic acid (time –15) and remained less until 30 minutes after washing off the ^{14}C–oleic acid (Figure 3F). The TG level in cellular pellets was greater in the *Mfge8*$^{-/-}$ and *αvβ3/αvβ5*$^{-/-}$ enterocytes as compared with WT controls 60 and 120 minutes

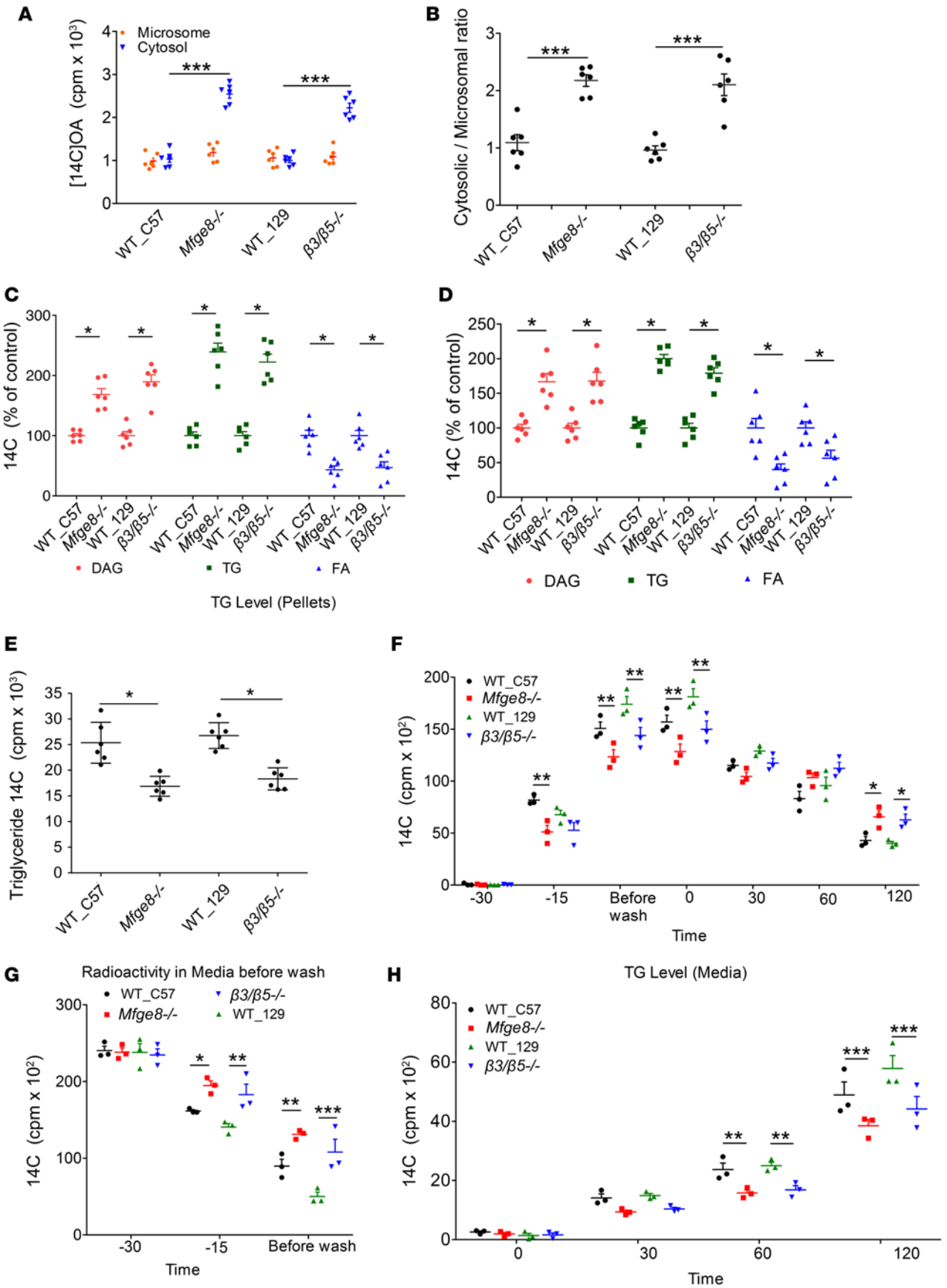
A
[14C]OA (cpm x 10³)
Microsome
Cytosol
***
***
WT_C57
Mfge8-/-
WT_129
β3/β5-/-
B
Cytosolic / Microsomal ratio
***
***
C
14C (% of control)
DAG
TG
FA
TG Level (Pellets)
D
14C (% of control)
DAG
TG
FA
E
Triglyceride 14C (cpm x 10³)
F
14C (cpm x 10²)
WT_C57
Mfge8-/-
WT_129
β3/β5-/-
Before wash
Time
G
Radioactivity in Media before wash
14C (cpm x 10²)
Time
H
TG Level (Media)
14C (cpm x 10²)
Time

Figure 3. Accumulation of cytoplasmic lipid droplets in *Mfge8*$^{-/-}$ and *αvβ3/αvβ5*$^{-/-}$ mice after a dietary fat challenge. (**A** and **B**) ^{14}C signal in the cytoplasmic versus microsomal compartments 2 hours after gavage with ^{14}C–oleic acid expressed as absolute radioactive counts (**A**) or as ratio of cytosolic to microsomal radioactivity (**B**). *n* = 6. (**C**) Incorporation of radiolabel into triglyceride (TG), diacylglycerol (DAG), and fatty acids (FA) in primary enterocytes isolated from the proximal jejunum 2 hours after gavage with ^{14}C-triolein. Lipids were resolved by TLC. The distribution of ^{14}C in the different lipid species is expressed as a percentage of total ^{14}C counts, with levels in WT cells set at 100%. *n* = 6. (**D**) Incorporation of ^{14}C into TG, DAG, and FA in primary enterocytes isolated from the proximal jejunum incubated for 30 minutes with bile salt micelles containing ^{14}C–oleic acid ([^{14}C]OA). Lipids were isolated by TLC 1.5 hours after removal of bile salt micelles. *n* = 6. (**E**) Incorporation of radiolabel in TG secreted into the media of primary enterocytes after 30 minutes of incubation with bile salt micelles containing [^{14}C]OA, followed by a 1.5-hour incubation with fresh media**.** *n* = 5. (**F**) Incorporation of ^{14}C into TG in primary enterocytes incubated with [^{14}C]OA-containing micelles followed by washing off micelles and a 2-hour incubation with fresh media. Lipids were resolved by TLC and the TG level is shown at time –30 (30 minutes before washing), –15, immediately before washing, and 0 (immediately after washing), 30, 60, and 120 minutes after wash. *n* = 3. (**G**) Total radioactivity in the media of primary enterocytes incubated with bile salt micelles containing [^{14}C]OA 30, 15, and 0 minutes before washing and replacing with fresh media. (**H**) Incorporation of [^{14}C]OA in TG secreted into the media of primary enterocytes after 30 minutes of incubation with bile salt micelles containing [^{14}C]OA. Lipids were resolved by TLC and the TG level is shown at time 0, 30, 60, and 120 minutes after replacing media. Both female and male mice were used in **A** and **B**, and female mice were used for the remaining panels. **P* < 0.05, ***P* < 0.01, ****P* < 0.001. Paired data were analyzed by Student's *t* test and group data were analyzed by 1-way ANOVA followed by a post-hoc Bonferroni test for multiple comparisons and expressed as the mean ± SEM.

after washing off the ^{14}C–oleic acid. The radiolabel signal in the media was greater in *Mfge8*$^{-/-}$ and *αvβ3/αvβ5*$^{-/-}$ enterocytes beginning at time –15 and before the wash step, consistent with a defect in uptake of radiolabeled fatty acid (Figure 3G). After washing off the ^{14}C–oleic acid micelles, TG levels in the media were less at 60 and 120 minutes in *Mfge8*$^{-/-}$ and *αvβ3/αvβ5*$^{-/-}$ enterocytes, consistent with a defect in chylomicron secretion (Figure 3H). Taken together, these data indicate that disruption of the Mfge8-integrin axis impedes absorption of FFAs and the FFAs that are successfully absorbed are trapped intracellularly as neutral lipids.

Fatty acids are released from cytoplasmic lipid droplets through the activity of TG hydrolases (16). Therefore, we evaluated whether enterocyte TG hydrolase activity was reduced in *Mfge8*$^{-/-}$ and *αvβ3/αvβ5*$^{-/-}$ mice. We first measured TG hydrolase activity in the jejunum of mice 2 hours after gavage with ^{14}C-triolein. Hydrolase activity was significantly reduced in *Mfge8*$^{-/-}$ and *αvβ3/αvβ5*$^{-/-}$ mice as compared with WT controls (Figure 4A). Furthermore, treatment of Caco-2 cells with recombinant Mfge8 (rMfge8) significantly increased hydrolase activity (Figure 4B). Treatment with an rMfge8 construct (RGE) with a single amino acid mutation (8, 21) changing the RGD sequence to RGE (and thereby preventing integrin binding) had no significant effect on TG hydrolase activity (Figure 4B). Treatment of Caco-2 with αv, β3, or β5 integrin–blocking antibodies significantly reduced hydrolase activity while treatment with a control β1 integrin–blocking antibody had no effect (Figure 4B). To mechanistically link Mfge8 and the αvβ3 and αvβ5 integrins, we evaluated the ability of rMfge8 to increase TG hydrolase activity in the presence of integrin-blocking antibodies. In both *Mfge8*$^{-/-}$ and WT primary enterocytes, rMfge8 did not increase TG hydrolase activity in the presence of αv, β3, or β5 subunit blockade, while it did increase uptake in the presence of β1-blocking antibody (Figure 4C). Furthermore, rMfge8 did not increase TG hydrolase activity in primary enterocytes from *αvβ3/αvβ5*$^{-/-}$ mice (Figure 4D). These data indicate that retention of cytoplasmic lipid droplets with disruption of the Mfge8-integrin axis is due to reduced TG hydrolase activity.

We next evaluated whether the effect of the Mfge8-integrin axis on hydrolase activity was specific for enterocytes. TG hydrolase activity was unaffected in primary hepatocytes and adipocytes from *Mfge8*$^{-/-}$ and *αvβ3/αvβ5*$^{-/-}$ mice (Supplemental Figure 5, A and B). Furthermore, white adipose tissue and liver TG levels 2 hours after i.p. administration of 200 μl of olive oil and intralipid fat emulsion were significantly lower in *Mfge8*$^{-/-}$ and *αvβ3/αvβ5*$^{-/-}$ mice (Supplemental Figure 5, C and D). Taken together, these data indicate that the effect of the Mfge8-integrin axis on TG hydrolase activity and intracellular lipid processing is specific for enterocytes.

We have previously shown that Mfge8 regulates uptake of FFAs through a PI3 kinase/mTORC2–dependent pathway (9). Therefore, we examined whether this signaling pathway mediated the effect of Mfge8 on enterocyte TG hydrolase activity. Indeed, inhibition of PI3 kinase with wortmannin prevented rMfge8 from increasing Caco-2 hydrolase activity (Figure 4E). siRNA knockdown of RICTOR (Figure 4F), the kinase of the mTORC2 complex, reduced baseline Caco-2 cell TG hydrolase activity and prevented the ability of rMfge8 to increase TG hydrolase activity (Figure 4G). Control siRNA had no effect on the ability of rMfge8 to increase TG hydrolase activity. These data indicate that the Mfge8-integrin axis increases TG hydrolase activity through a PI3 kinase/mTORC2 pathway (Figure 5).

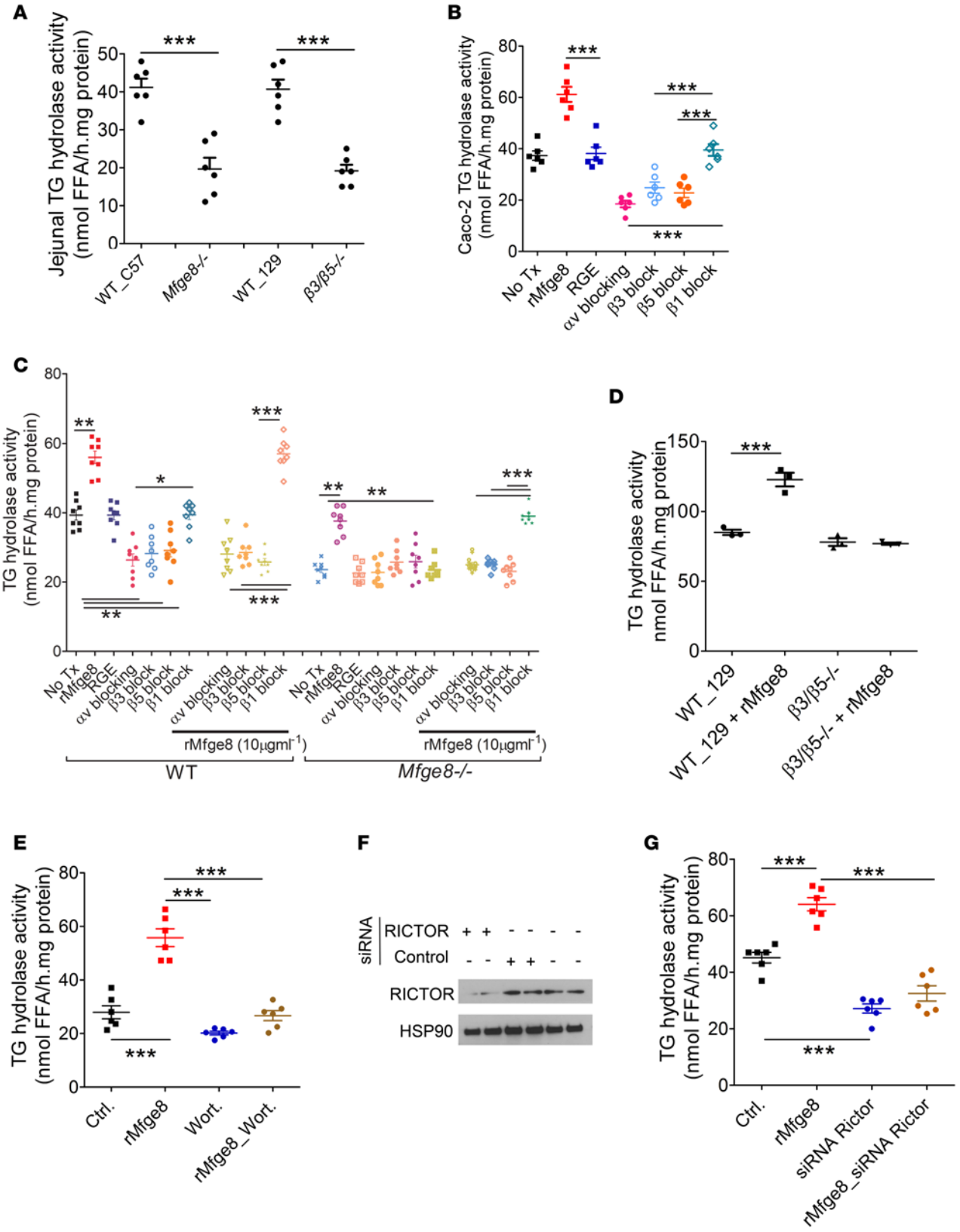

Figure 4. Impaired triglyceride (TG) hydrolase activity in enterocytes from *Mfge8*$^{-/-}$ and *αvβ3/αvβ5*$^{-/-}$ mice. (**A**) TG hydrolase activity in the proximal jejunal segments of mice measured 2 hours after olive oil gavage. *n* = 5–6. (**B**) Effect of rMfge8 (10 μg/ml), RGE (an rMfge8 mutant that does not bind integrin, 10 μg/ml), and integrin-blocking (αv, β3, β5, and β1; 5 μg/ml) antibodies on TG hydrolase activity in the Caco-2 cell line. *n* = 4–6. (**C**) Effect of rMfge8 (10 μg/ml) in the absence and presence of integrin-blocking (αv, β3, β5, and β1; 5 μg/ml) antibodies on TG hydrolase activity in the proximal jejunal enterocytes of mice. *n* = 5–7. (**D**) Effect of rMfge8 (10 μg/ml) on TG hydrolase activity in the primary enterocytes from *αvβ3/αvβ5*$^{-/-}$ mice. *n* = 3.

(**E**) TG hydrolase activity in Caco-2 cells treated with wortmannin (100 ng/ml) and rMfge8. $n = 4–6$. (**F**) Western blot of differentiated Caco-2 cells after incubation with siRNA targeting RICTOR or control siRNA. (**G**) TG hydrolase activity in differentiated Caco-2 cells treated with siRNA targeting RICTOR or control siRNA and rMfge8. $n = 4–6$. Female mice were used for panel **A**. Both female and male mice were used in panel **C**. $^{**}P < 0.01$, $^{***}P < 0.001$. Paired data were analyzed by Student's *t* test and group data were analyzed by 1-way ANOVA followed by a post-hoc Bonferroni test for multiple comparisons and expressed as the mean ± SEM. Ctrl., control; No Tx, no treatment.

Discussion

In this work, we show that Mfge8 and the αvβ3 and αvβ5 integrins promote enterocyte hydrolysis of cytoplasmic lipid droplets by activating intracellular TG hydrolase activity. Mice deficient in Mfge8 or the αvβ3 and αvβ5 integrins retain dietary TG in cytoplasmic lipid droplets after both acute and chronic dietary fat challenge. The accumulation of cytoplasmic lipid droplets is coupled with impaired TG hydrolase activity in vitro and in vivo. The observed increase in enterocyte neutral lipid content after fat loading of *Mfge8*$^{-/-}$ and *αvβ3/αvβ5*$^{-/-}$ mice is in contrast with what we previously reported under basal and fasting conditions. Enterocyte TG content in *Mfge8*$^{-/-}$ and *αvβ3/αvβ5*$^{-/-}$ mice under normal diet or fasting conditions is reduced as compared with WT mice (9). We believe this reduction represents a combination of impaired absorption of FFAs from the normal diet and impaired uptake of serum fatty acids under fasting conditions, leading to reduced intracellular TG content. Therefore, the importance of the Mfge8-integrin axis in regulating cytoplasmic lipid droplet homeostasis is evident only in the presence of an acute or chronic fat challenge.

The current knowledge of lipid droplet metabolism is primarily from work done in adipocytes and hepatocytes, and has identified a number of molecules that associate with and regulate hydrolysis of lipid-droplet TGs. ATGL, CGI-58, the perilipin family of proteins, and G0S2 are established lipid droplet–associated proteins with roles in TG hydrolysis (15, 16, 22, 23). Whether these molecules play a dominant role in enterocyte TG hydrolysis is unclear. Mouse lines with enterocyte-specific knockout of ATGL or CGI-58 have a modest reduction in enterocyte TG hydrolase activity (15, 24). In fact, the residual TG hydrolase activity in both of these knockout mouse lines is proportionally dominant relative to the amount of hydrolase activity lost due to ATGL/CGI-58 knockdown (15, 24). These data suggest that there is an as of yet unidentified hydrolase(s) that mediates the bulk of cytoplasmic lipid droplet breakdown in enterocytes. In fact, the approximately 50% reduction in TG hydrolase activity we report here in *Mfge8*$^{-/-}$ and *αvβ3/αvβ5*$^{-/-}$ mice is quantitatively greater than that seen with enterocyte-specific ATGL or CGI-58 knockdown. Identification of an enterocyte TG hydrolase(s) that is regulated by Mfge8 is currently an area of active investigation in our laboratory.

Another interesting observation from our data is the increased expression of DGAT2 in *Mfge8*$^{-/-}$ mice on an HFD. A recent paper demonstrates that intestinal overexpression of DGAT2 leads to enhanced enterocyte TG secretion (25). The reduced secretion of TG by *Mfge8*$^{-/-}$ enterocytes raises the intriguing possibility that DGAT2 expression is increased as a compensatory mechanism to normalize TG secretion.

The importance of enterocyte lipid storage under conditions of high dietary fat intake is evident by the stronger correlation of postprandial lipemia with cardiovascular disease as compared with fasting serum lipid levels (1, 2). In particular, chylomicron remnants are thought to contribute to atherosclerotic disease by rapidly penetrating the arterial wall (26, 27). By retaining absorbed dietary TG as cytoplasmic lipid droplets, enterocytes have the ability to limit the extent of postprandial lipemia (28). TG in cytoplasmic lipid droplets is hydrolyzed by intracellular lipases releasing FFAs, which are then re-esterified, and packaged as part of chylomicrons for peripheral distribution. The mechanisms that regulate hydrolysis of cytoplasmic lipid droplets in particular in relation to ingestion of dietary fat are unknown.

Mfge8 has been shown to regulate inflammation in multiple organ systems (7, 29) including the gastrointestinal tract (30–33). In most instances, Mfge8 deficiency promotes inflammation either due to impaired apoptotic cell clearance (7) or through direct effects of Mfge8 on inflammatory signaling after integrin ligation (8, 21). In the intestine, Mfge8 has been shown to ameliorate inflammation in models of DSS- and TNBS-induced experimental colitis (30, 31, 34). Obesity is characterized by chronic adipose and systemic inflammation (35). In our previous work, we found that *Mfge8*$^{-/-}$ placed on an HFD were protected from systemic and adipose tissue inflammation due to their impaired ability to take up and store FFAs. Whether interactions between Mfge8 and intestine-resident immune cells may directly or indirectly modulate the ability of enterocytes to hydrolyze cytoplasmic lipid droplets is an interesting possibility that cannot be ruled out based on the data presented in this manuscript.

While the precise role of Mfge8 in human metabolism remains unclear, there is evidence to support a

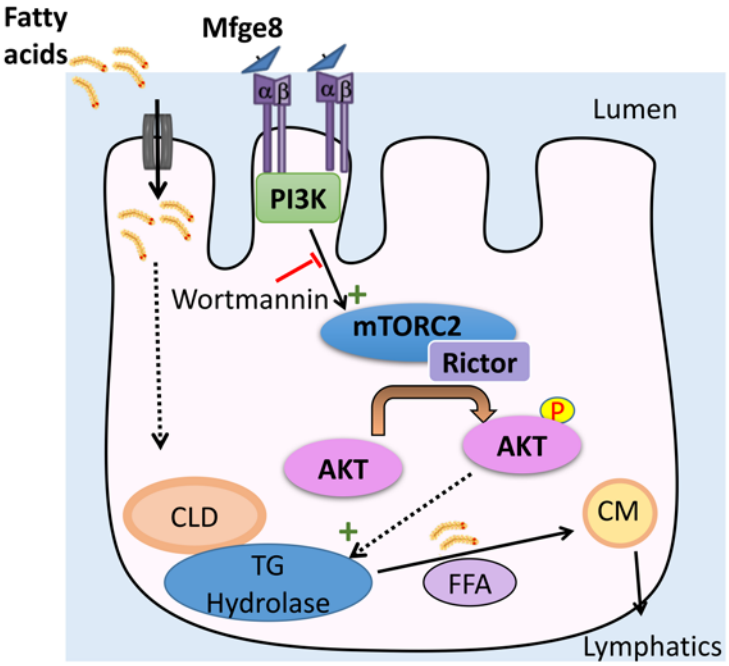

Figure 5. Model to describe the mechanism by which Mfge8 regulates triglyceride (TG) hydrolysis. Mfge8 binding to the αvβ3 and αvβ5 integrins on the surface of enterocytes activates a PI3 kinase/mTORC2 pathway that increases TG hydrolase activity. The increase in TG hydrolase activity leads to the release of free fatty acids from cytoplasmic lipid droplets which can then be utilized for chylomicron production. CLD, cytoplasmic lipid droplet; CM, chylomicron; FFA, free fatty acids.

role for the Mfge8/integrin pathway in obesity. Adipose tissue obtained from obese humans has increased expression of Mfge8 and the αv and β5 integrin subunits (36). The gene for *MFGE8* is in a region linked with susceptibility to obesity and eating behaviors in humans (37, 38). Additionally, circulating Mfge8 concentrations correlate with the degree of hemoglobin glycosylation and are elevated in diabetics, a disease with markedly increased prevalence in obese subjects (39, 40).

The work presented here identifies Mfge8 and the αvβ3 and αvβ5 integrins as a key pathway regulating enterocyte processing of dietary fats. Together with our previously published work (9), our findings indicate that Mfge8 ligation of the αvβ3 and αvβ5 integrins on enterocytes triggers activation of a PI3 kinase/mTORC2 complex that results in uptake of luminal FFAs (9) and release of FFAs from cytoplasmic lipid droplets, thereby providing 2 sources of fatty acids for chylomicron production. Preferential trafficking of TG from newly absorbed fatty acids to cytoplasmic lipid droplets has been suggested based on human studies looking at the fatty acid composition of chylomicrons secreted after sequential ingestion of fat-rich meals with different fatty acid compositions (6). Therefore, the Mfge8 pathway may serve as a critical link that coordinates the process by which newly absorbed fatty acids are deposited in cytoplasmic lipid droplets while fat stored from previous meals is mobilized for chylomicron production. From a therapeutic viewpoint, this pathway could be targeted to reduce chylomicron secretion as well as reduce fat absorption.

Methods

Mice. Six- to 8-week-old age- and sex-matched mice were used for all studies. The sex of mice for each experiment is included in the figure legends. *Mfge8*$^{-/-}$ mice were purchased from RIKEN, are in the C57BL/6 background, and have been extensively characterized (41). C57BL/6 WT mice were used as controls for all studies with *Mfge8*$^{-/-}$ mice. *αvβ3/αvβ5*$^{-/-}$ mice are in the 129SVEV background and have been previously characterized (42). WT mice in the 129SVEV background were used as controls for studies with *αvβ3/αvβ5*$^{-/-}$ mice.

Triolein and cholesterol gavage. Six- to 8-week-old sex-matched mice were fasted for 4 hours. Mice had access to water but not food for the remainder of the experiment. In Figure 1, A–E, an oral gavage of 200 μl olive oil was administered. In Figure 1, F and G, 200 μl olive oil containing 3.5 μCi ^{14}C-triolein was administered by intragastric gavage. Prior to and 30, 60, 90, and 120 minutes after olive oil/^{14}C-triolein administration, 10 μl blood was drawn from the tail vein. Two hours after the oil bolus, the mice were euthanized. The small intestine was washed, excised and divided into 5 equal-length segments in relation to the stomach and labeled segments 1–5. Segments 2 and 3 represented the jejunum. Segment 2, the proximal jejunum, was used for the data in Figure 1F, H, and I, Figure 2, A–C, Figure 3, A–D, and Figure 4, A and C. Segments 2 and 3 (representing the whole jejunum) were used for enterocyte isolation (Figure 1A).

Enterocyte isolation. Primary enterocytes were collected by harvesting the jejunal segment as described above from euthanized mice, emptying the luminal contents, washing with 115 mM NaCl, 5.4 mM KCl, 0.96 mM NaH_2PO_4, 26.19 mM $NaHCO_3$, and 5.5 mM glucose buffer at pH 7.4, and gassing for 30 minutes with 95% O_2 and 5% CO_2 (43). The lumen was then filled with buffer containing 67.5 mM NaCl, 1.5 mM KCl, 0.96 mM NaH_2PO_4, 26.19 mM $NaHCO_3$, 27 mM sodium citrate, and 5.5 mM glucose at pH 7.4, saturated with 95% O_2 and 5% CO_2, and incubated in a bath containing oxygenated saline at 37°C with constant shaking. After 15 minutes, luminal solutions were discarded and the intestines filled with buffer

containing 115 mM NaCl, 5.4 mM KCl, 0.96 mM NaH_2PO_4, 26.19 mM $NaHCO_3$, 1.5 mM EDTA, 0.5 mM dithiothreitol, and 5.5 mM glucose at pH 7.4, saturated with 95% O_2 and 5% CO_2, and placed in saline as described above. After 15 minutes, the luminal contents were centrifuged (500 *g*, 5 minutes, room temperature) and the pellets resuspended in DMEM saturated with 95% O_2 and 5% CO_2.

Adipocyte and hepatocyte isolation. Primary mouse adipocytes were obtained from epididymal fat pads by collagenase digestion in Krebs-HEPES (KRBH) buffer followed by filtering through a 100-μm strainer, which was subsequently washed with an additional 7.5 ml KRBH buffer. Adipocytes were allowed to float to the top of the mixture for 5 minutes, after which the solution under the adipocyte layer was removed with a syringe. Adipocytes were washed with 10 ml KRBH and again allowed to float to the surface, after which the solution was again removed. This process was repeated 3 times and the cells resuspended and counted from 0.5–1.0 ml.

Primary hepatocytes were obtained by perfusing the liver through the portal vein with calcium-free buffer (0.5 mM EDTA, HBSS without Ca^{2+} and Mg^{2+}) and then perfusing with collagenase (3.5 U/ml collagenase II from Worthington, 25 mM HEPES, HBSS with Ca^{2+} and Mg^{2+}). Parenchymal cells were purified with Percoll buffer (90% Percoll [Sigma-Aldrich]), 1× PBS) at low-speed centrifugation (500 *g* for 10 minutes). Cells were plated in collagen I–coated dishes and cultured at 37°C in a humidified atmosphere of 95% O_2 and 5% CO_2 in growth medium (44).

Lipid analysis. Primary enterocytes were plated and pulsed with a labeling mixture (DMEM containing 0.4 mM sodium taurocholate, 0.52 mM sodium taurodeoxycholate, 0.29 mM phosphatidylcholine, 0.45 mM oleic acid, 0.16 mM 1-oleoyl-*rac*-glycerol, 0.05 mM cholesterol) containing 3.3 μCi/ml ^{14}C–oleic acid for 30 minutes at 37°C and 5% CO_2. Cells were washed, and fresh media without ^{14}C was added to the cells. After 1.5 hours, lipids were extracted using the method of Folch et al. (45) from enterocytes and media, resuspended in chloroform, and resolved by TLC in hexane/isopropyl ether/glacial acetic acid 60:40:4 (v/v/v). After the different lipid species were identified according to standards, bands corresponding to the lipids indicated in Figure 3 were scraped, incubated overnight in Scintilene scintillation fluid (Thermo Fisher Scientific), and quantified by scintillation spectroscopy. The distribution of ^{14}C in the different lipid classes is expressed as a percentage of counts, with levels in WT cells taken as 100% (in Figure 3, C and D), and radioactivity level (in Figure 3, F and G).

Lipid content. Serum TG and FFA concentrations were measured using commercially available kits (Sigma-Aldrich and Wako, respectively). TG content of the intestine (proximal jejunum) was quantified in Figure 2, B and C, that of primary enterocytes isolated from the jejunum in Figure 1A, and that of fecal samples, liver, and epididymal white adipose tissue (eWAT) as described previously (9, 46, 47), and normalized to the weight of the tissue or proteins. For the experiments in Figure 1, B and C, we treated mice with or without an i.p. injection of the lipoprotein lipase inhibitor Triton WR-1339 (Sigma-Aldrich, 200 mg per kg body weight) 30 minutes before olive oil gavage, with subsequent measurement of TG concentrations. In Supplemental Figure 5, C and D, TG level of the liver and eWAT was measured after i.p. injecting 8-hour-fasted mice with 200 μl of Intralipid (Sigma-Aldrich) 20% (v/v) fat emulsion.

Subcellular fractionation. Two hours after ^{14}C-triolein gavage, primary enterocytes were isolated from the jejunal segment of the euthanized mice. Enterocytes were washed with Ca^{++}/Mg^{++}–free HBSS and then were lysed in a disruption buffer containing 25 mM Tris/HCl (pH 7.4) 100 mM KCl, 1 mM EDTA, 5 mM ethyleneglycotetraacetic acid (EGTA), and a protease inhibitor cocktail. Cell lysates were mixed with an equal volume of disruption buffer containing 1.08 M sucrose after disrupting by nitrogen and sonication. After centrifugation at 1500 *g* for 10 minutes to pellet nuclei, the supernatant was transferred to a 12-ml ultracentrifugation tube and overlaid sequentially with 2.0 ml each of 0.27 M sucrose buffer, 0.135 M sucrose buffer, and Top solution (25 mM Tris-HCl, 1 mM EDTA, and 1 mM EGTA, pH 7.4). Following centrifugation at 150,500 *g* for 60 minutes, 8 fractions of 1.5 ml each were collected from top to bottom: the buoyant lipid bodies (fractions 1 and 2), the mid-zone (fractions 3 and 4) between lipid bodies and cytosol, and the cytosol (fractions 5–8). The microsomal pellet (fraction 9) and nuclei (fraction 10) were washed and resuspended in 1.5 ml Top solution. The protein content of each fraction was measured by micro BCA assay using bovine serum albumin as a standard. The activities of lactate dehydrogenase and sulfatase C were measured as a cytosolic and microsomal marker, respectively (48). After ultracentrifugation, aliquots of each fraction were counted for radioactivity to determine lipid labeling in subcellular compartments.

TG hydrolase activity assay. TG hydrolase activity was assayed as previously described (49). Briefly, the intestinal protein was isolated from mice. One hundred micrograms of protein in 100 μl of 100 mM potas-

sium phosphate lysis buffer was incubated with 100 μl TG substrate (25 nmol triolein/assay and 40,000 cpm/nmol ^{14}C-triolein; PerkinElmer) and 35.5 μg mixed micelles of phosphatidylcholine and phosphatidylinositol (3:1, w/w), respectively. After incubation at 37°C for 1 hour, the reaction was terminated by adding 3.25 ml methanol/chloroform/heptane (10:9:7, v/v/v) and 1 ml 100 mM potassium carbonate (pH 10.5 with boric acid). After centrifugation (800 *g*, 15 minutes, 4°C), the radioactivity in 1 ml of the upper phase was determined by liquid scintillation counting.

Cell culture and treatment. Caco-2 cells were differentiated by maintaining confluent monolayers in minimum essential medium supplemented with 10% FBS at 37°C under 5% CO_2 on 3.0-μm transwell inserts (3415, Costar) for 3 weeks. In experiments using function-blocking antibodies, we added 5 μg/ml antibodies against mouse integrin α_v (clone RMV-7, Abcam) (50), β_3 (clone 2C9.G2; BD Biosciences) (51), β_5 (clone ALULA, provided by A. Atakilit, UCSF) (52), β1 (clone HA2/5; BD Biosciences, raised against rat with crossreactivity with mouse) (53) and human integrins α_v (clone L230, provided by A. Atakilit) (54), β_3 (clone Axum-2) (55), β_5 (clone ALULA), and β1 (clone P5D2) to the cells for 15 minutes, after which rMfge8 (10 μg/ml) was added for another 30 minutes. For PI3 kinase inhibition, cells were incubated with 100 ng/ml wortmannin (Sigma-Aldrich) for 20 minutes, after which rMfge8 was added to the cells for another 30 minutes. Cells were then used for the TG hydrolase activity assay.

Flow cytometry. Primary enterocytes were harvested as described above and pelleted by centrifuging at 200 *g*. Cells were stained for annexin V and with PI following the manufacturer's protocol using a FITC Annexin V Apoptosis Detection Kit with PI (640914, BioLegend).

siRNA. Caco-2 cells were maintained in minimum essential medium supplemented with 10% FBS at 37°C under 5% CO_2. After 2 weeks of differentiation in transwell plates, cells were transfected with 100 nM RICTOR siRNA (ON-TARGETplus Human RICTOR, 253260, Thermo Fisher Scientific) or controls (ON-TARGETplus Control siRNA, Human, Thermo Fisher Scientific) in antibiotic- and norepinephrine-free culture medium using Lipofectamine 2000 (Invitrogen). SMARTpool siRNA was used, which is a mixture of 4 siRNAs provided as a single reagent. Six hours later, the supplemented medium containing 10% FBS was added. The TG hydrolase assay was conducted 48 hours after transfection.

MTTP activity assay. Small pieces (0.1 g) of liver and proximal jejunum (1 cm) were homogenized in low-salt buffer (1 mM Tris-HCl, pH 7.6, 1 mM EGTA, and 1 mM $MgCl_2$) and centrifuged, and supernatants were used for protein determination and the MTTP assay using a commercial kit (Chylos, Inc.) (56).

Oil Red O staining and immunofluorescence staining. Mice were fasted for 4 hours before administration of olive oil gavage and for 12 hours after 3 weeks on an HFD. Two hours after gavage and immediately after 12 hours of fasting, the mice were euthanized, and the small intestine was divided into 5 segments. Segment 2 was cut longitudinally, fixed in z-fix (catalog 170, Anatech LTD) at 4°C for 3 hours, and immersed in 30% sucrose overnight. Samples were embedded in OCT and frozen in chilled isopropanol on dry ice. Frozen sections (10 μm) were prepared, stained with Oil Red O and hematoxylin, and visualized by light microscopy at ×200 magnification. For immunofluorescence staining, 5-μm paraffin-embedded sections were cleared with xylene, rehydrated, boiled for 20 minutes, and passively cooled for 20 minutes in 10 mM sodium citrate (pH 6) for antigen retrieval. Sections were blocked in Tris-buffered saline (TBS) with 0.5% Tween 20 and 10% goat serum. Antibody against perilipin 3 (catalog abs482, Millipore) was applied at 1:250 dilution followed by Alexa Fluor 488 (A-11008, Molecular Probes) at 1:300 in TBS with 0.5% Tween 20 and 10% goat serum. Sections were mounted in Fluoromount G (0100-01, SouthernBiotech). Images were captured by a Leica point scanner using a Leica TCS SPE confocal microscope with an ACS APO 63× Oil CS objective lens at room temperature with Leica Type F Immersion Liquid (11513859). Images were processed with Photoshop CS5 software (Adobe).

Western blot. Mice were gavaged with 200 μl of olive oil. Two hours after gavage, jejunal segments were harvested as described above and homogenized in cold RIPA buffer (50 mM Tris HCl pH 7.5, 150 mM NaCl, 1% NP-40, 1% sodium deoxycholate, 0.1% SDS) supplemented with complete miniprotease and phosphatase inhibitor cocktail (Pierce). Lysates were incubated at 4°C with gentle rocking for 30 minutes, sonicated on ice for 30 seconds, and then centrifuged at 13,000 *g* for 15 minutes at 4°C. Protein concentration was determined by the Bradford assay (Bio-Rad). Protein (20 μg) was resolved by SDS-PAGE in 7.5% gels (Bio-Rad) and transblotted onto polyvinylidene fluoride membranes (Millipore). Membranes were incubated with antibody against ApoB (1:1,000; Abcam, ab20737) and β-actin (1:5,000; Sigma-Aldrich, A5441).

RNA extraction and quantitative RT-PCR. Mice were given HFD for 2 weeks. Total RNA was purified from mouse jejunum by guanidinium thiocyanate/phenol/chloroform extraction. Briefly, tissues were

homogenized in TRIsure (Bioline BIO-38033) and mixed with 1-bromo-3-chloropropane. After centrifugation, the aqueous phase was mixed with 2-propanol to precipitate RNA. The precipitate was pelleted by centrifugation and washed with ethanol. RNA was analyzed with a NanoDrop 2000 (Thermo Fisher Scientific) to determine purity and quantity and 1 μg of RNA was used for first-strand cDNA synthesis (Quanta 95048). Quantitative RT-PCR was performed using SensiFast SYBR green (Bioline) on the CFX384 Real Time PCR system (Bio-Rad). Data are presented as relative expression by the comparative threshold method using 36B4 as the internal control. Primer pairs are listed in Supplemental Figure 6.

rMfge8. rMfge8 and the RGE construct consisted of murine cDNA of Mfge8 (long isoform) fused with the human FC domain and expressed in High Five cells as previously described (8). The RGE construct contains a point mutation changing the RGD sequence to RGE. These recombinant constructs were used for all studies, except for the data in Figure 4D. Commercial rMfge8 from R&D Systems was used for the studies presented in Figure 4D.

Statistics. One-way ANOVA was used to make comparisons between multiple groups. When the ANOVA comparison was statistically significant ($P < 0.05$), further pairwise analysis was performed using a Bonferroni *t* test. A 2-sided Student's *t* test was used for comparisons between 2 groups. For analysis of weight gain over time in mice, a 2-way ANOVA for repeated measures was used. GraphPad Prism 6.0 was used for all statistical analyses, and the data are presented as the mean ± SEM.

Study approval. All experiments were approved by the Institutional Animal Care and Use Committee of UCSF.

Author contributions

AKS designed and performed all experiments and wrote the manuscript. DG contributed to the TG hydrolase assays, Western blots, and helped write the manuscript. AH was responsible for histological analysis and aided with the in vivo mouse experiments. MP provided significant intellectual contribution and helped with writing the manuscript. JI performed MTTP activity assays. MH aided with experimental design and data analysis. KA designed and oversaw all experiments and wrote the manuscript.

Acknowledgments

This work was supported in part by an Award from the American Heart Association Western States Affiliate and the American Brain Foundation to AKS (14POST18580033), awards from the American Heart Association (15GRNT25080286) and the National Institutes of Health (DK110098) to KA, and awards from the National Institutes of Health (DK-81879 and DK-46900) to MH. We would like to thank S. Layer for ongoing inspiration.

Address correspondence to: Kamran Atabai, Department of Medicine, University of California San Francisco, Cardiovascular Research Institute - MC: 3118, 555 Mission Bay Boulevard South, Room 252R, San Francisco, California 94158-9001, USA. Phone: 415.514.1159; E-mail: Kamran.Atabai@UCSF.edu.

1. Patsch JR, et al. Relation of triglyceride metabolism and coronary artery disease. Studies in the postprandial state. *Arterioscler Thromb*. 1992;12(11):1336–1345.
2. Miller M, et al. Triglycerides and cardiovascular disease: a scientific statement from the American Heart Association. *Circulation*. 2011;123(20):2292–2333.
3. Zhu J, Lee B, Buhman KK, Cheng JX. A dynamic, cytoplasmic triacylglycerol pool in enterocytes revealed by ex vivo and in vivo coherent anti-Stokes Raman scattering imaging. *J Lipid Res*. 2009;50(6):1080–1089.
4. Karpe F, Steiner G, Uffelman K, Olivecrona T, Hamsten A. Postprandial lipoproteins and progression of coronary atherosclerosis. *Atherosclerosis*. 1994;106(1):83–97.
5. Federico LM, Naples M, Taylor D, Adeli K. Intestinal insulin resistance and aberrant production of apolipoprotein B48 lipoproteins in an animal model of insulin resistance and metabolic dyslipidemia: evidence for activation of protein tyrosine phosphatase-1B, extracellular signal-related kinase, and sterol regulatory element-binding protein-1c in the fructose-fed hamster intestine. *Diabetes*. 2006;55(5):1316–1326.
6. Fielding BA, Callow J, Owen RM, Samra JS, Matthews DR, Frayn KN. Postprandial lipemia: the origin of an early peak studied by specific dietary fatty acid intake during sequential meals. *Am J Clin Nutr*. 1996;63(1):36–41.
7. Atabai K, et al. Mfge8 is critical for mammary gland remodeling during involution. *Mol Biol Cell*. 2005;16(12):5528–5537.
8. Atabai K, et al. Mfge8 diminishes the severity of tissue fibrosis in mice by binding and targeting collagen for uptake by macrophages. *J Clin Invest*. 2009;119(12):3713–3722.
9. Khalifeh-Soltani A, et al. Mfge8 promotes obesity by mediating the uptake of dietary fats and serum fatty acids. *Nat Med*. 2014;20(2):175–183.

10. Khalifeh-Soltani A, et al. α8β1 integrin regulates nutrient absorption through an Mfge8-PTEN dependent mechanism. *Elife*. 2016;5.
11. Abumrad NA, Davidson NO. Role of the gut in lipid homeostasis. *Physiol Rev*. 2012;92(3):1061–1085.
12. Thiam AR, Farese RV, Walther TC. The biophysics and cell biology of lipid droplets. *Nat Rev Mol Cell Biol*. 2013;14(12):775–786.
13. Drover VA, et al. CD36 mediates both cellular uptake of very long chain fatty acids and their intestinal absorption in mice. *J Biol Chem*. 2008;283(19):13108–13115.
14. Drover VA, et al. CD36 deficiency impairs intestinal lipid secretion and clearance of chylomicrons from the blood. *J Clin Invest*. 2005;115(5):1290–1297.
15. Xie P, et al. Intestinal Cgi-58 deficiency reduces postprandial lipid absorption. *PLoS ONE*. 2014;9(3):e91652.
16. Zimmermann R, et al. Fat mobilization in adipose tissue is promoted by adipose triglyceride lipase. *Science*. 2004;306(5700):1383–1386.
17. Schweiger M, et al. Adipose triglyceride lipase and hormone-sensitive lipase are the major enzymes in adipose tissue triacylglycerol catabolism. *J Biol Chem*. 2006;281(52):40236–40241.
18. Lass A, et al. Adipose triglyceride lipase-mediated lipolysis of cellular fat stores is activated by CGI-58 and defective in Chanarin-Dorfman Syndrome. *Cell Metab*. 2006;3(5):309–319.
19. Haemmerle G, et al. Defective lipolysis and altered energy metabolism in mice lacking adipose triglyceride lipase. *Science*. 2006;312(5774):734–737.
20. Lee B, Zhu J, Wolins NE, Cheng JX, Buhman KK. Differential association of adipophilin and TIP47 proteins with cytoplasmic lipid droplets in mouse enterocytes during dietary fat absorption. *Biochim Biophys Acta*. 2009;1791(12):1173–1180.
21. Kudo M, et al. Mfge8 suppresses airway hyperresponsiveness in asthma by regulating smooth muscle contraction. *Proc Natl Acad Sci USA*. 2013;110(2):660–665.
22. Sahu-Osen A, et al. CGI-58/ABHD5 is phosphorylated on Ser239 by protein kinase A: control of subcellular localization. *J Lipid Res*. 2015;56(1):109–121.
23. Cantley JL, et al. CGI-58 knockdown sequesters diacylglycerols in lipid droplets/ER-preventing diacylglycerol-mediated hepatic insulin resistance. *Proc Natl Acad Sci U S A*. 2013;110(5):1869–1874.
24. Obrowsky S, et al. Adipose triglyceride lipase is a TG hydrolase of the small intestine and regulates intestinal PPARα signaling. *J Lipid Res*. 2013;54(2):425–435.
25. Uchida A, Slipchenko MN, Eustaquio T, Leary JF, Cheng JX, Buhman KK. Intestinal acyl-CoA:diacylglycerol acyltransferase 2 overexpression enhances postprandial triglyceridemic response and exacerbates high fat diet-induced hepatic triacylglycerol storage. *Biochim Biophys Acta*. 2013;1831(8):1377–1385.
26. Tomkin GH, Owens D. Abnormalities in apo B-containing lipoproteins in diabetes and atherosclerosis. *Diabetes Metab Res Rev*. 2001;17(1):27–43.
27. Vine DF, Glimm DR, Proctor SD. Intestinal lipid transport and chylomicron production: possible links to exacerbated atherogenesis in a rodent model of the metabolic syndrome. *Atheroscler Suppl*. 2008;9(2):69–76.
28. Robertson MD, et al. Mobilisation of enterocyte fat stores by oral glucose in humans. *Gut*. 2003;52(6):834–839.
29. Cui T, et al. Milk fat globule epidermal growth factor 8 attenuates acute lung injury in mice after intestinal ischemia and reperfusion. *Am J Respir Crit Care Med*. 2010;181(3):238–246.
30. Kusunoki R, et al. Role of milk fat globule-epidermal growth factor 8 in colonic inflammation and carcinogenesis. *J Gastroenterol*. 2015;50(8):862–875.
31. Zhang Y, Brenner M, Yang WL, Wang P. Recombinant human MFG-E8 ameliorates colon damage in DSS- and TNBS-induced colitis in mice. *Lab Invest*. 2015;95(5):480–490.
32. Zhao QJ, Yu YB, Zuo XL, Dong YY, Li YQ. Milk fat globule-epidermal growth factor 8 is decreased in intestinal epithelium of ulcerative colitis patients and thereby causes increased apoptosis and impaired wound healing. *Mol Med*. 2012;18:497–506.
33. Aziz MM, et al. MFG-E8 attenuates intestinal inflammation in murine experimental colitis by modulating osteopontin-dependent alphavbeta3 integrin signaling. *J Immunol*. 2009;182(11):7222–7232.
34. Otani A, et al. Intrarectal administration of milk fat globule epidermal growth factor-8 protein ameliorates murine experimental colitis. *Int J Mol Med*. 2012;29(3):349–356.
35. Ferrante AW. Obesity-induced inflammation: a metabolic dialogue in the language of inflammation. *J Intern Med*. 2007;262(4):408–414.
36. Henegar C, et al. Adipose tissue transcriptomic signature highlights the pathological relevance of extracellular matrix in human obesity. *Genome Biol*. 2008;9(1):R14.
37. Rankinen T, et al. The human obesity gene map: the 2005 update. *Obesity (Silver Spring)*. 2006;14(4):529–644.
38. Twito T, Madeleine D, Perl-Treves R, Hillel J, Lavi U. Comparative genome analysis with the human genome reveals chicken genes associated with fatness and body weight. *Anim Genet*. 2011;42(6):642–649.
39. Cheng M, et al. Correlation between serum lactadherin and pulse wave velocity and cardiovascular risk factors in elderly patients with type 2 diabetes mellitus. *Diabetes Res Clin Pract*. 2012;95(1):125–131.
40. Yu F, et al. Proteomic analysis of aorta and protective effects of grape seed procyanidin B2 in db/db mice reveal a critical role of milk fat globule epidermal growth factor-8 in diabetic arterial damage. *PLoS One*. 2012;7(12):e52541.
41. Asano K, et al. Masking of phosphatidylserine inhibits apoptotic cell engulfment and induces autoantibody production in mice. *J Exp Med*. 2004;200(4):459–467.
42. Reynolds LE, et al. Enhanced pathological angiogenesis in mice lacking beta3 integrin or beta3 and beta5 integrins. *Nat Med*. 2002;8(1):27–34.
43. Anwar K, Iqbal J, Hussain MM. Mechanisms involved in vitamin E transport by primary enterocytes and in vivo absorption. *J Lipid Res*. 2007;48(9):2028–2038.
44. Huang P, et al. Induction of functional hepatocyte-like cells from mouse fibroblasts by defined factors. *Nature*. 2011;475(7356):386–389.
45. Folch J, Lees M, Sloane Stanley GH. A simple method for the isolation and purification of total lipides from animal tissues. *J Biol Chem*. 1957;226(1):497–509.
46. Uchida A, et al. Reduced triglyceride secretion in response to an acute dietary fat challenge in obese compared to lean mice.

Front Physiol. 2012;3:26.
47. Kim KY, et al. Parkin is a lipid-responsive regulator of fat uptake in mice and mutant human cells. *J Clin Invest*. 2011;121(9):3701–3712.
48. Yu W, Cassara J, Weller PF. Phosphatidylinositide 3-kinase localizes to cytoplasmic lipid bodies in human polymorphonuclear leukocytes and other myeloid-derived cells. *Blood*. 2000;95(3):1078–1085.
49. Chandak PG, et al. Efficient phagocytosis requires triacylglycerol hydrolysis by adipose triglyceride lipase. *J Biol Chem*. 2010;285(26):20192–20201.
50. Takahashi K, et al. A murine very late activation antigen-like extracellular matrix receptor involved in CD2- and lymphocyte function-associated antigen-1-independent killer-target cell interaction. *J Immunol*. 1990;145(12):4371–4379.
51. Ashkar S, et al. Eta-1 (osteopontin): an early component of type-1 (cell-mediated) immunity. *Science*. 2000;287(5454):860–864.
52. Su G, et al. Integrin alphavbeta5 regulates lung vascular permeability and pulmonary endothelial barrier function. *Am J Respir Cell Mol Biol*. 2007;36(3):377–386.
53. Zovein AC, et al. Beta1 integrin establishes endothelial cell polarity and arteriolar lumen formation via a Par3-dependent mechanism. *Dev Cell*. 2010;18(1):39–51.
54. Thomas GJ, Hart IR, Speight PM, Marshall JF. Binding of TGF-beta1 latency-associated peptide (LAP) to alpha(v)beta6 integrin modulates behaviour of squamous carcinoma cells. *Br J Cancer*. 2002;87(8):859–867.
55. Su G, et al. Absence of integrin αvβ3 enhances vascular leak in mice by inhibiting endothelial cortical actin formation. *Am J Respir Crit Care Med*. 2012;185(1):58–66.
56. Athar H, Iqbal J, Jiang XC, Hussain MM. A simple, rapid, and sensitive fluorescence assay for microsomal triglyceride transfer protein. *J Lipid Res*. 2004;45(4):764–772.